Improving snow processes in the Noah land model

Zhuo Wang,[1] Xubin Zeng,[1] and Mark Decker[1]

Received 23 December 2009; revised 21 June 2010; accepted 24 June 2010; published 22 October 2010.

[1] Snow is one of the most crucial land surface processes over middle and high latitudes. A widely known deficiency of the Noah land model as used in the National Centers for Environmental Prediction (NCEP) operational models and the Weather Research and Forecasting model (WRF) at the National Center for Atmospheric Research is that snowmelt occurs much too early. Through detailed diagnostics of the Noah output over the high-altitude Niwot Ridge forest site (40.03°N, 105.55°W) and a boreal forest site (53.9°N, 104.7°W), six deficiencies in Noah model physics are identified along with improved formulations that (1) consider the vegetation shading effect on snow sublimation and snowmelt; (2) consider under-canopy resistance; (3) revise the ground heat flux computation when snow is deep; (4) revise the momentum roughness length computation when snow is present; (5) revise the snow density computation near 0°C; and (6) increase the maximum iteration number from five to 30 in the turbulence computation. These revisions significantly improve Noah simulations of all snow processes such as snow water equivalent (SWE), snow depth, and sensible and latent heat fluxes over these two forest sites. The revisions were also evaluated (without tunings) with an independent forest site and a grassland site, further confirming the robust and positive impacts of these revisions on Noah snow simulations. These modifications maintain the Noah model structure and do not introduce new prognostic variables, allowing easy implementation into NCEP operational models and into WRF. Furthermore, they are found to be as good as, or slightly better than, a much more complicated land model in the snow simulation over the three forest sites.

Citation: Wang, Z., X. Zeng, and M. Decker (2010), Improving snow processes in the Noah land model, *J. Geophys. Res.*, *115*, D20108, doi:10.1029/2009JD013761.

1. Introduction

[2] Snow has an important impact on climate at all spatial scales because of its high albedo, low thermal conductivity, and low roughness length [*Slater et al.*, 2001]. Snow is also important for the hydrological cycle because of the accumulation of water in the snowpack in winter and its subsequent release during the springtime snowmelt [*Wang and Zeng*, 2009]. Timing of snowmelt also affects precipitation prediction over land in the following summer [e.g., *Vernekar et al.*, 1995]. Despite the importance of snow, modeling efforts indicate a large spread in the climatic response to snow cover change largely due to different snow treatments in models [*Anderson et al.*, 1976; *Jordan*, 1991; *Slater et al.*, 2001; *Qu and Hall*, 2006].

[3] Intercomparisons of various snow models of different complexities have been conducted in numerous previous studies [e.g., *World Meteorological Organization*, 1986; *Frei and Robinson*, 1998; *Slater et al.*, 2001; *Bowling et al.*, 2003; *Boone et al.*, 2004; *Etchevers et al.*, 2004; *Frei et al.*, 2005; *Feng et al.*, 2008; *Rutter et al.*, 2009; *Essery et al.*, 2009]. In particular, *Rutter et al.* [2009] recently evaluated the performance of a large number of snow models of varying complexities and purposes across a wide range of climatological, hydrometeorological, and forest canopy conditions. Their results indicate that there was no universal "best" model or subset of "better" models. Most models, including the Noah land model [*Mitchell et al.*, 2004] (see also http://gcmd.nasa.gov/records/NOAA_NOAH.html) are good in certain aspects, but not good in others.

[4] Noah is used as the land component in the regional and global weather forecasting models at the National Centers for Environmental Prediction (NCEP) and in the Weather Research and Forecasting model (WRF) at the National Center for Atmospheric Research (NCAR). Several research groups [e.g., *Jin et al.*, 1999; *Sheffield et al.*, 2003; *Ek et al.*, 2003; *Pan et al.*, 2003; *Mitchell et al.*, 2004; *Jin and Miller*, 2007; *Slater et al.*, 2007] have noticed that Noah has problems with snowmelt and snow sublimation. Early attempts to improve cold-season processes in Noah were made in an off-line mode by *Koren et al.* [1999] and during the PILPS 2d exercise [*Schlosser et al.*, 2000, *Slater et al.*, 2001]. For example, *Slater et al.* [2001] found that the early season ablation events were a significant source of the difference in snow water equivalent (SWE) among 21 land

[1]Department of Atmospheric Sciences, University of Arizona, Tucson, Arizona, USA.

0148-0227/10/2009JD013761

surface models. *Ek et al.* [2003] then tested their improvements in a coupled mode within the NCEP mesoscale Eta model and found that upgrading of snowpack and adding frozen soil physics were crucial in representing wintertime conditions. The previous cold biases in the wintertime low-level temperatures were partially mitigated by including patchy snow cover that allows greater surface heating and increased soil heat flux. Recently, *Livneh et al.* [2010] made some revisions in snow albedo, snow aging effect, and water-holding capacity of snow to improve the Noah simulation of snow processes.

[5] While the revisions from previous efforts improve the Noah snow simulations in their sensitivity tests, their impact on snow-related processes (e.g., net radiation, sensible and latent heat fluxes) were sometimes not reported [e.g., *Livneh et al.*, 2010]. For instance, while the increases of albedo would certainly reduce the energy available for snow sublimation and melt, it also reduces the net radiation flux that is balanced by ground heat flux, and latent and sensible heat fluxes (with the latter two closely coupled to atmospheric boundary layer processes). In particular, previous revisions did not explicitly consider three dominant physical processes associated with deep snow under dense boreal forest in spring [e.g., *Betts and Ball*, 1997]: (1) Surface albedo is low because snow is shaded by the forest canopy; (2) sublimation and melt of snow under canopy are small because most of the solar radiation cannot penetrate through the canopy; and (3) most of the net solar radiation is converted to sensible heat flux that drives a relatively deep atmospheric boundary layer.

[6] The questions are as follows: (1) Is it possible to robustly improve the Noah simulation of snow processes and other variables (e.g., latent and sensible heat fluxes) without changing the model structure (for easy operational implementation at NCEP)? (2) How good are such improvements in comparison with other land models using a more sophisticated model structure (e.g., with separate snow, canopy, and ground temperatures versus the single combined temperature of canopy, ground, and snow in Noah)? Building on extensive previous efforts on snow processes in Noah and other land models, the purpose of this paper is to directly address the first question and briefly address the second question by comparing our revisions in Noah with the NCAR Community Land Model (CLM3.5) [*Oleson et al.*, 2008].

[7] The snow processes in Noah and CLM3.5 as well as the observational data used in this study are summarized in section 2. The deficiencies in Noah snow processes and our suggested revisions are described in section 3, while their impacts on Noah modeling of snow processes are presented in section 4. Further discussions and conclusions are provided in section 5.

2. Model and Data Descriptions

2.1. Model Description

[8] The original OSU Land Model was developed in the 1980s [*Mahrt and Pan*, 1984]. It has evolved into the Noah land model through community efforts to simulate land surface temperature, snow depth, snow water equivalent (SWE), canopy water content, surface energy and water balance, as well as soil temperature and moisture [*Chen et al.*, 1996; *Ek et al.*, 2003; *Feng et al.*, 2008]. It is widely used in operational and research applications and can be run in a coupled or off-line mode. Detailed descriptions of the Noah formulations and development are provided elsewhere [*Koren et al.*, 1999; *Chen and Dudhia*, 2001; *Ek et al.*, 2003], and only a brief description of the equations related to our revisions is provided here. In this study, Noah version 2.7.1 as used in the NCEP Global Forecast System (GFS) is used.

[9] The Penman equation for surface energy balance [*Penman*, 1948; *Mahrt and Ek*, 1984] is used in Noah to compute latent heat flux, with other fluxes computed later [*Chen et al.*, 1997; *Slater et al.*, 2007]. Following *Koren et al.* [1999], Noah has four soil layers reaching a depth of 2 m in which frozen water is considered. It also contains a one-layer snow submodel that simulates SWE as the residual of snowfall minus the sum of snowmelt and sublimation. Snowfall occurs whenever there is nonzero precipitation and 2 m air temperature is less than 0°C. Snow melting occurs and melted water is removed as runoff when the temperature for canopy, ground, and snow is greater than the freezing point and SWE is greater than zero. Freezing occurs when the layer temperature is less than the freezing point and SWE is greater than zero.

[10] Potential evapotranspiration (E_p) is computed from the Penman equation [*Penman*, 1948; *Mahrt and Ek*, 1984] as

$$E_p = \frac{\Delta}{1+\Delta}(R_{\text{net}} - G) + \frac{\rho L_v}{r_a(1+\Delta)}(q^* - q) \tag{1a}$$

$$\Delta = \frac{0.622}{p}\frac{L_v}{c_p}\frac{d\,e^*(T)}{dT} \tag{1b}$$

$$R_{\text{net}} = SW_{\text{net}} + LW_{\text{net}}, \tag{1c}$$

where R_{net} is the net radiative flux gained by the surface, SW_{net} is the net solar radiation, LW_{net} is the net longwave radiation, G is the ground heat flux, ρ is the surface air density, L_v is the latent heat of condensation, c_p is the specific heat of air, r_a is the aerodynamic resistance [$r_a = 1/(C_h\,u)$] with C_h being the turbulent exchange coefficient and u the wind speed, q^* is the saturated atmospheric specific humidity, e^* is the saturated vapor pressure, p is surface pressure, and T is near-surface air temperature.

[11] The snow sublimation rate (E_{sn}) is determined by

$$E_{sn} = E_p \cdot F_{sn}, \tag{2a}$$

$$F_{sn} = \alpha_s \frac{W}{W_{\text{max}}}\exp[-\alpha_s(W/W_{\text{max}})] + \frac{1}{W_{\text{max}}}\exp(-\alpha_s), \tag{2b}$$

where F_{sn} is the fractional snow coverage of the model grid cell, W is the SWE, W_{max} is the vegetation type-dependent maximum SWE for full snow fraction, and α_s is a distribution shape parameter.

[12] Snow accumulation/ablation parameterizations of the Noah model are based on mass and energy balance in the snowpack. The change in snowpack SWE is balanced by the input snowfall, and output snowmelt and snow sublimation. The snowmelt rate (M_s) is determined by

$$M_s = \frac{R_{es}}{L_f} = \frac{1}{L_f}(R_{net} - G - LH - SH - F_1 - F_2), \tag{3}$$

where R_{es} is the energy available for the snowmelt, L_f is the latent heat of fusion, LH is the latent heat flux, SH is the sensible heat flux, F_1 is the heat flux from newly accumulating precipitation, and F_2 is the freezing rain latent heat flux.

[13] The soil, vegetation, and snow are modeled as a single unit over the entire grid box in Noah [*Slater et al.*, 2007], which is one of the factors affecting the snow simulation. In contrast CLM3.5, which is the land component of the NCAR Community Climate System Model (CCSM [*Collins et al.*, 2006]), considers the soil, vegetation, and snow separately. The CLM3.5 snow submodel contains up to five snow layers depending on the total snow depth [*Dai et al.*, 2003; *Oleson et al.*, 2004]. It also considers three different snow fractions that have clear physical meanings [*Wang and Zeng*, 2009]: (1) the horizontal snow cover fraction as a function of the soil roughness length and used in the ground albedo computation; (2) the canopy intercepted snow fraction as a function of the leaf and stem area indexes and primarily used in the intercepted snow sublimation computation; and (3) the vertical burial fraction as a function of snow depth and canopy height (both top and bottom) that is used to adjust the leaf and stem area indexes projected above the snow [*Oleson et al.*, 2004]. Some previous studies [e.g., *Wang and Zeng*, 2009; *Lawrence and Chase*, 2009] demonstrated that CLM3.5 can reasonably simulate land processes (including snow processes) over different regions of the world using global in situ data and satellite data.

2.2. Data

[14] The observational data over three forests sites and a grass site are used in this study: the Niwot Ridge forest site (40.03°N, 105.55°W), the boreal forest site (53.9°N, 104.7°W), the Fraser forest site (39.53°N, 105.53°W), and the Valdai grass site (57.6°N, 33.1°E).

2.2.1. Niwot Ridge Forest Site

[15] First, we use the data collected from 1 July 2006 to 30 June 2007 at the Niwot Ridge AmeriFlux site (for AmeriFlux description, see *Hollinger and Wofsy* [1997]; data are available at http://public.ornl.gov/ameriflux/) in the Colorado Front Range (40.03°N, 105.55°W). The depth of snow accumulation at this site is extremely variable and is influenced by the interaction of high wind velocities and topography [*Cline*, 1996]. The high elevation and exposure of the Niwot Ridge and the typically dry atmospheric conditions result in large clear-sky atmospheric transmissivity, large solar insolation, low downward longwave radiation, low air temperatures, and high wind velocities. The location of the precipitation gauge is in a windy site without natural vegetation or topographic barriers to act as a wind shield. For these reasons, accurate measurements of precipitation are particularly difficult at this site [*Williams et al.*, 1998]. Calculating the actual deposition of snow at a point in alpine areas is also difficult because wind transport of snow can cause under-sampling or over-sampling of the actual precipitation amount. Flux and meteorological measurements were made from a 26 m tall scaffolding tower. Details of this study site are given by *Turnipseed et al.* [2002, 2003] and *Monson et al.* [2002]. The meteorology of this area has been well documented in previous studies [*Barry*, 1973; *Brazel and Brazel*, 1983; *Parrish et al.*, 1990].

[16] The precipitation data from this AmeriFlux site differ from those over an adjacent Snow Telemetry (SNOTEL) site. It is well recognized that snowfall is a major source of uncertainty in the land model simulation of SWE [e.g., *Slater et al.*, 2001]. For this reason, precipitation data (particularly in winter and over complex terrain) have been corrected in previous land modeling studies [e.g., *Mote et al.*, 2003; *Feng et al.*, 2008]. In this study, the low snowfall observed over this site (probably due to wind transport) is not suitable for land modeling studies because the observed maximum SWE there is even higher than the total accumulated snowfall. We also checked the data over the SNOTEL site and found that the SWE data from SNOTEL are less than the accumulated snowfall over the site. Therefore we simply adjusted the Ameriflux precipitation data used to force the Noah and CLM3.5 simulations according to the SNOTEL data during the snowfall period.

2.2.2. Boreal Forest Site

[17] The Boreal Ecosystem-Atmosphere Study (BOREAS) is a large-scale international interdisciplinary experiment in the boreal forest of Canada. The BOREAS study region covered most of Saskatchewan and Manitoba, containing northern study areas and southern study areas (SSA) within which process study sites were located [*Sellers et al.*, 1997]. A more detailed description of the site locations, site environments, and instrumentation is given by *Shewchuk* [1997]. In this study, we use the airborne fluxes and meteorology (AFM) and tower fluxes (TF) data over the old jack pine (OJP) site (53.9°N, 104.7°W) in the SSA from 1 July 1994 to 30 June 1995. Because only snow depth was measured over this site, we also use the daily 0.25° snow depth and SWE data over North America from the Canadian Meteorological Centre (CMC) [*Brown et al.*, 2003]. The gridded snow depth data combine in situ daily observations from ~8000 U.S. cooperative and Canadian climate stations and first-guess fields with an optimum interpolation scheme developed by *Brasnett* [1999] and used operationally at CMC [*Niu and Yang*, 2007]. These snow depth data and a snow model are then used to estimate SWE [*Brown et al.*, 2003].

2.2.3. Fraser Forest Site

[18] The observational data from 1 October 2002 to 30 September 2003 over the Fraser forest site (39.53°N, 105.53°W) are available at http://nsidc.org/data/nsidc-0172.html. This site is located in the Rocky Mountains of Colorado, and is part of the Small Regional Study Area (SRSA) of the Cold Land Processes Field Experiment (CLPX). The SRSA contains six towers for measuring meteorological variables [*Elder and Goodbody*, 2004]. The tower at St. Louis Creek evergreen pine forest site is used here due in part to its elevation of approximately 2700 m above sea level and its vegetation cover. The elevations of other towers are generally higher, and short vegetation and evergreen forests coexist there. Also, a total of six snow pits were dug near the St. Louis tower to provide measurements of snow depth and snow water equivalent at six time periods [*Cline et al.*, 2004].

[19] Two primary corrections to the forcing data were made. First, despite ventilation, the downward longwave and shortwave radiation measurements were degraded by snow accumulation on the sensors during storms. Visual inspection of the data showed that during storm periods, the measured shortwave radiation would oscillate from 850 to 50 and back to 850 W/m^2 in 30 min. To remove such

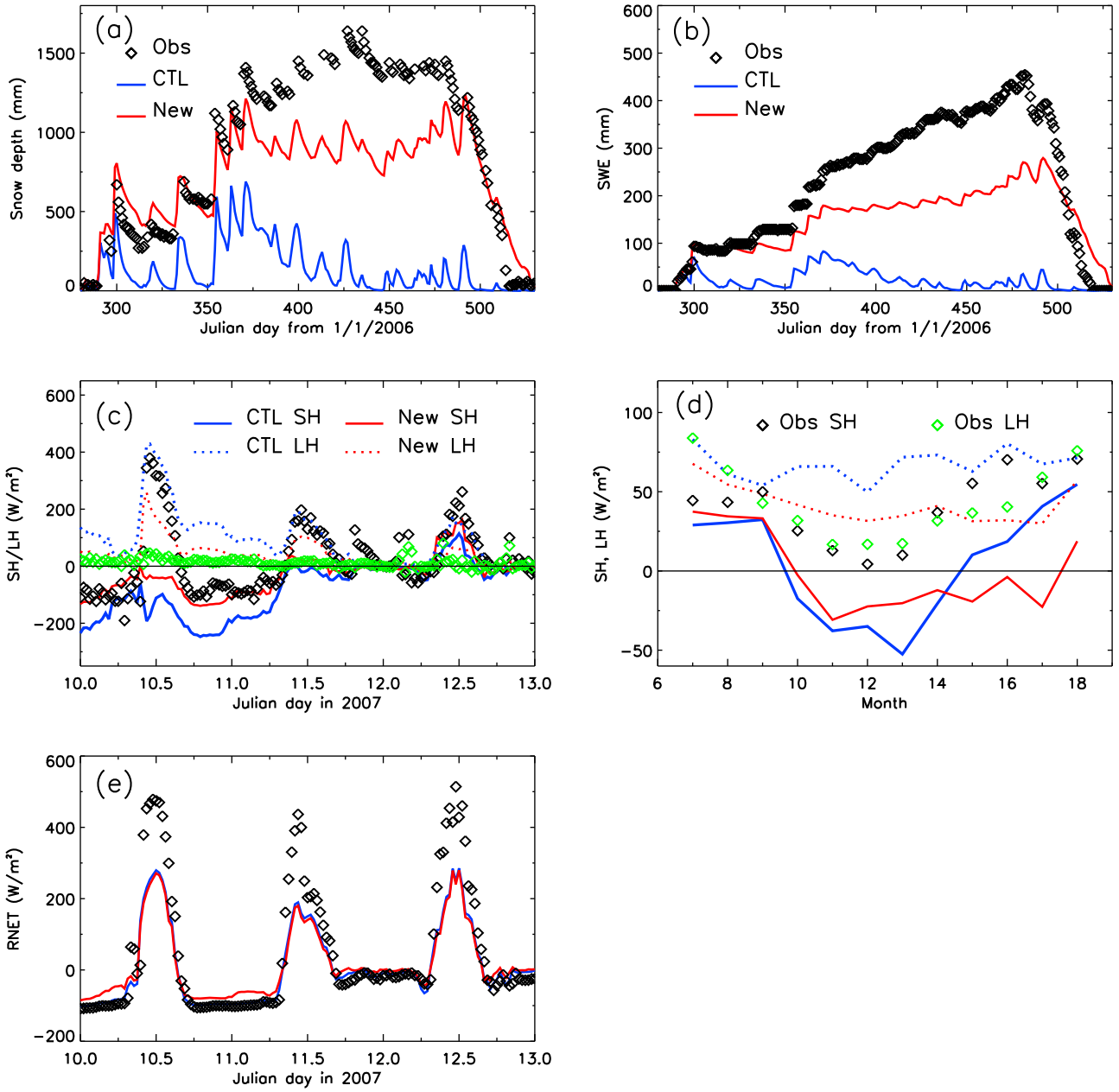

Figure 1. Comparison of Noah control and new simulations with observed data of (a) daily average snow depth; (b) daily average snow water equivalent (SWE); (c) sensible (*SH*) and latent (*LH*) heat fluxes at each time step (half hour); (d) monthly sensible and latent heat fluxes; and (e) net radiative flux over the Niwot Ridge site (40.03°N, 105.55°W).

unphysical behaviors, a nine-point filter was used to smooth the longwave and shortwave radiation (with the restriction that the shortwave radiation is zero before sunrise or after sunset). Second, precipitation was not measured at this particular tower and the total precipitation hourly data from the Modern Era Retrospective-analysis for Research and Applications (MERRA) are used (available at http://gmao.gsfc.nasa.gov/research/merra/intro.php). However, the accumulated precipitation data during the snow accumulation period are much less than the measured SWE (figure not shown), similar to the situation over the Niwot Ridge site. Therefore the precipitation data were adjusted during the snow season using the measured SWE to ensure that the adjusted accumulated precipitation is slightly larger than the measured SWE (figure not shown).

2.2.4. Valdai Grass Site

[20] Over the Valdai grass site (57.6°N, 33.1°E), the soil and vegetation data are taken from PILPS 2d [*Slater et al.*, 2001]. The meteorological data set during the period of 1966–1983 eight times per day (0000, 0300, 0600, 0900, 1200, 1500, 1800, and 2100 LT) are used to force the land model. The data at this site have been used in many land model simulations, and details of the data were described by *Vinnikov et al.* [1996] and *Schlosser et al.* [2000]. SWE was measured every 10 days over this site.

Table 1. Description of Seven Noah Simulations With Our Revisions in Section 3 Over the Niwot Ridge Forest Site (40.03°N, 105.55°W)

Experiment	Description
1	control run
2	Exp. 1 + vegetation shading effect; equations (4) and (5)
3	Exp. 2 + under canopy resistance; equation (6)
4	Exp. 3 + adjusted ground heat flux; equation (8)
5	Exp. 4 + revised z0m under snow condition; equations (9) and (10)
6	Exp. 5 + adjusted snow density near 0° C; equations (11) and (12)
7	Exp. 6 + maximum iteration number of 30

[21] Over each of these four sites, Noah (or CLM3.5) is run from arbitrary initial conditions for 10 years by cycling the first year's atmospheric forcing data. Then the model state after the 10 year spin-up period is used as the initial condition to run the model for the whole period with observed forcing data.

3. Deficiencies in Noah Snow Simulations and Suggested Revisions

[22] To better understand the deficiencies in the Noah simulation of snow processes, we systematically evaluated the model output of all relevant variables (e.g., snowmelt, snow sublimation, evaporation, transpiration, SWE, snow depth and density, soil moisture, and runoff for the water cycle) over the Niwot Ridge site (40.03°N, 105.55°W), which is dominated by evergreen needleleaf forest. In this way, we are able to identify several deficiencies in the current Noah model physics and to suggest revisions.

[23] The main deficiencies in Noah snow simulations are demonstrated in Figure 1 by comparing Noah simulations with observed data over the Niwot Ridge forest site (40.03°N, 105.55°W). Both snow depth and SWE are too low compared with observations (Figures 1a and 1b) due to overestimates of latent heat flux (and hence snow sublimation) in late winter and early spring (Figure 1d). Furthermore, the downward sensible heat flux is overestimated under very stable conditions relative to observation (e.g., on 11 January 2007 in Figure 1c). To reduce these Noah deficiencies, several revisions are proposed here and their effects are evaluated using model experiments in Table 1.

3.1. Shading Effect of Vegetation

[24] In winter, for deep snow with full ground snow cover ($F_{g,sn}$ = 100%) under trees, little net radiation $R_{\rm net}$ (or net shortwave radiation $SW_{\rm net}$) reaches snow because forest canopies shade underlying snow from both direct and diffuse solar radiation [*Essery et al.*, 2009]. Since Noah does not consider this shading effect and computes a single temperature (T_1) for vegetation, bare soil, and the snow layer, it would overestimate net solar radiation, and hence $R_{\rm net}$ in equation (1). This leads to the overestimation in potential evapotranspiration (E_p) (equation (1)) and hence in snow sublimation (equation (2a)) and snowmelt (equation (3)).

[25] Although the shading effect on snow albedo is considered in Noah by using satellite-based (or vegetation type-dependent) maximum snow albedo data, it is not considered in the computation of snow sublimation and snowmelt. Here we consider the vegetation shading effect on snow sublimation and melt by introducing the fraction of vegetation with snow below (F_{vb})

$$F_{vb} = GVF \cdot F_{g,sn}(1 - F_{\rm bur}), \tag{4a}$$

$$F_{g,sn} = W/W_{cr,g}, \tag{4b}$$

$$F_{\rm bur} = \frac{H_{sn} - Z_{\rm bot}}{Z_{\rm top} - Z_{\rm bot}}, \tag{4c}$$

where GVF is the green vegetation fraction, $F_{g,sn}$ is the fraction of ground covered with snow and is between 0 and 1, W is the SWE, $W_{cr,g}$ = 0.02 m is the critical SWE for fully snow-covered ground, $F_{\rm bur}$ is the snow burial fraction and is between 0 and 1, H_{sn} is the snow depth, and $Z_{\rm top}$ and $Z_{\rm bot}$ are the canopy top and bottom heights, respectively, prescribed as a function of vegetation type. For grasses and crops without strong trunks, $Z_{\rm top}$ is taken as 0.2 m in equation (4c) following *Wang and Zeng* [2009]. To avoid confusion, it is worth noting that four different snow fractions are used in this study: Fraction F_{vb} is that of vegetation with snow below, $F_{g,sn}$ is the fraction of ground covered with snow, $F_{\rm bur}$ is the snow burial fraction, and F_{sn} is the fractional snow coverage in the model grid cell. These fractions are defined in equations (4a), (4b), (4c), and (2b), respectively.

[26] Vegetation shading should affect both the solar and longwave radiation reaching the under-canopy snow. However, the effect on solar radiation is generally more important during the day. Therefore we introduce a new net radiation $R_{\rm net,new}$ (=$SW_{\rm net,new}$ + $LW_{\rm net}$) with the new net shortwave radiation ($SW_{\rm net,new}$) as the weighted average between the vegetation shaded fraction F_{vb} from equation (4) and the nonshaded fraction $1 - F_{vb}$ as

$$R_{\rm net,new} = (0.44 \cdot SW\downarrow \cdot \gamma) \cdot F_{vb} + (1-\alpha)SW\downarrow \cdot (1 - F_{vb}) + LW_{\rm net}, \tag{5a}$$

$$R_{\rm net,new} = Max\left[R_{\rm net,new},\ R_{\rm net} - Min(D_{\max},\ 0.5(1-\alpha)SW\downarrow)\right], \tag{5b}$$

where $SW\downarrow$ is the downward solar radiation, $\gamma = \exp(-LAI)$ with LAI being leaf area index. The factor 0.44 = (1 − 0.5)(1 − 0.13) is used because the net solar radiation absorbed by under-canopy snow can be approximated by $(1-\alpha_v)(1-\alpha_{g,sn}) \cdot {\rm SW}\downarrow \cdot \exp(-LAI)$ with vegetation albedo $\alpha_v \approx 0.13$ and under-canopy snow albedo $\alpha_{g,sn} \approx 0.5$, $D_{\max}$ = 250 W/m^2, and α is the grid cell average albedo computed in Noah [*Wang and Zeng*, 2010]. $R_{\rm net,new}$ is then used to replace $R_{\rm net}$ in the computation of potential evapotranspiration in equation (1a) and hence the snow sublimation in equation (2a) and snowmelt in equation (3). Furthermore, using $R_{\rm net,new}$ to replace $R_{\rm net}$ is implemented only when the following conditions are all met: where $R_{\rm net} > R_{\rm net,new}$; when there is energy for snowmelt ($R_{es} > 0$) in equation (3); during daytime; and when the top soil layer temperature $T_{\rm soil(1)} < 0$°C or ($T_{\rm soil(1)} > 0$°C and $T_{\rm air} > 0$°C). In addition, the change of net radiation should not change R_{es} in equation (3) from positive (for snowmelt) to negative (for freezing). In other words, if $R_{es} \le R_{\rm net} - R_{\rm net,new}$, we take $R_{\rm net,new} = R_{\rm net} - R_{\rm es}$.

[27] As mentioned earlier, most of the solar heating for forests with underlying snow is used to heat the atmospheric boundary layer through sensible heat [e.g., *Betts and Ball*, 1997]. Therefore, to maintain the energy balance in Noah,

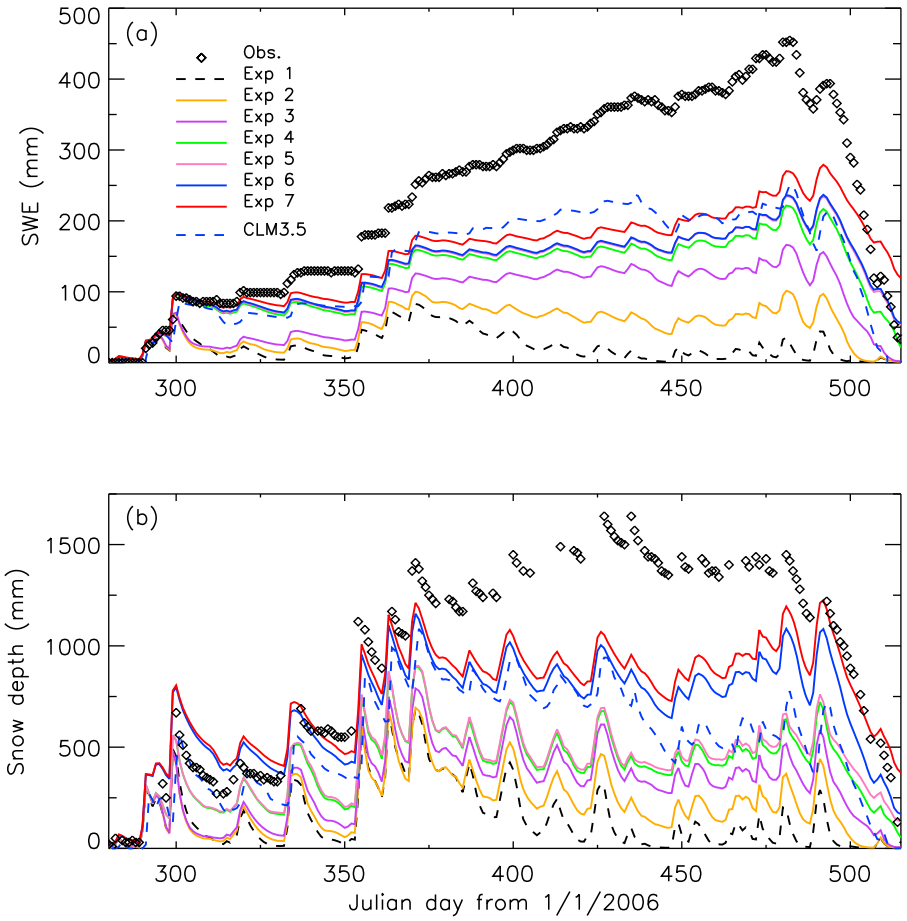

Figure 2. Comparison of daily mean SWE and snow depth from the seven experimental simulations in Table 1 and from NCAR Community Land Model (CLM) 3.5 over the Niwot Ridge site.

the simplest way is to add ($R_{net} - R_{net,new}$) to the sensible heat flux (*SH*). Because *SH* is usually less than 350 W/m^2 over forest sites with underlying snow based on data analysis (e.g., over the Niwot Ridge site or other sites of *Decker and Zeng* [2009]) and is also constrained by the solar energy absorbed by the surface (vegetation, snow, and soil), we restrain ($R_{net} - R_{net,new}$) to be less than 250 W/m^2 (which is a portion of the above peak *SH* value) and less than half of the solar energy absorbed by the surface (vegetation, snow, and soil) in absolute value in equation (5b). Sensitivity tests show that results are not much affected if slightly different values are used (figure not shown). Similarly, the values of $\alpha_v \approx 0.13$ and $\alpha_{g,sn} \approx 0.5$ are estimated from satellite data analysis [e.g., *Wang et al.*, 2004], and results are insensitive to their exact values (figure not shown).

[28] The shortwave and longwave radiative transfer through the vegetation and snow is much more complicated than the above simplification. The canopy, snow, and bare soil temperatures should be separately computed (as in CLM3.5) because they might differ significantly. However, we intend to maintain the Noah coding structure for easy implementation and hence decide to keep the single temperature for canopy, snow, and bare soil in Noah. The consequence is that we have to introduce equation (5) with a few parameters that cannot be fully justified. The usefulness of our revisions, including equation (5), will be demonstrated by comparing the Noah results with our revisions with those from CLM3.5.

[29] Figure 2 compares the daily mean SWE and snow depth with different revisions in the order shown in Table 1 over the Niwot Ridge site. Consideration of the vegetation shading effects on snowmelt and sublimation (Exp. 2) improves the SWE simulation relative to the Noah control run (Exp. 1). The snow depth is also improved slightly compared with observations (Figure 2b).

3.2. Under-Canopy Resistance

[30] Figure 1c shows that when the air temperature (T_a) is greater than surface skin temperature (T_1) with strong winds (i.e., under weakly stable conditions), downward *SH* is significantly overestimated in Noah on 10 January 2007. Further diagnostics indicate that this is caused by a too small aerodynamic resistance $r_a = 1/(C_h\, u)$.

[31] Under stable conditions (i.e., $T_a > T_1$), we consider the under-canopy resistance (r_u) as

$$r_u = r_{u,\max} \cdot GVF \cdot F_{g,sn} \cdot \mathrm{Min}\left(\frac{T_a - T_1}{5}, 1\right) \times [1 - \exp(-LAI_{\mathrm{eff}})], \tag{6a}$$

$$LAI_{\mathrm{eff}} = LAI(1 - F_{\mathrm{bur}}), \tag{6b}$$

where $r_{u,\max}$ is 100 *s/m*, $F_{g,sn}$ is ground snow fraction defined in equation (4b), F_{bur} is the snow burial fraction in equation (4c). Formulation (6a) was motivated by the study of *Sakaguchi and Zeng* [2009]. Figure 2 shows that the consideration of the under-canopy resistance in Noah (Exp. 3) leads to improved SWE and snow depth simulations.

3.3. Ground Heat Flux Adjustment

[32] The ground heat flux under snow condition is computed in Noah as

$$G = \left(T_1 - T_{\text{soil}(1)}\right) \cdot \frac{DF_1}{DTOT}, \tag{7a}$$

$$DTOT = \Delta Z_s + \Delta Z_{s1}, \tag{7b}$$

$$DF_1 = F_{sn}\frac{\Delta Z_s K_s + \Delta Z_{s1} K_{s1}}{\Delta Z_s + \Delta Z_{s1}} + (1 - F_{sn}) \cdot K_{s1}, \tag{7c}$$

where T_1 is the surface skin temperature, $T_{\text{soil}(1)}$ is the upper soil layer temperature, ΔZ_s is the snow depth, ΔZ_{s1} is the upper soil layer depth, K_{s1} and K_s are the thermal conductivities of the upper soil layer and snow layer, respectively, and F_{sn} is the snow cover fraction ($0 \le F_{sn} \le 1$) in equation (2b). *Ek et al.* [2003] provided a more detailed description about the G computation.

[33] Under deep snow conditions, $F_{sn} \sim 1$, $DF_1 \sim K_s$, and $DTOT \sim \Delta Z_s$ so that G becomes very small. This would increase the energy available and hence increase the snowmelt in equation (3) during the day. In reality, G does exist and plays a role in the computation of T_1 over deep snow.

[34] To remove the Noah deficiency in computing G under deep snow condition (which is primarily caused by using a single bulk snow layer in Noah), we revise the ground heat flux by limiting the minimum value of $DF_1/DTOT$ used in equation (7a) by

$$G = \left(T_1 - T_{\text{soil}(1)}\right) \cdot \text{Max}(DD_{\min},\ DF_1/DTOT), \tag{8}$$

where $DD_{\min} = 7\ \text{W m}^{-2}\ K^{-1}$, as motivated by the European Centre for Medium-Range Weather Forecasts (ECMWF) land model (see http://www.ecmwf.int/research/ifsdocs/CY28r1). Figure 2 shows that equation (8) (Exp. 4) improves the Noah simulation of SWE and snow depth.

3.4. Roughness Length Adjustment Under Snow Conditions

[35] The roughness length for momentum (z_{0m}) in Noah is not adjusted under snow conditions. This may be reasonable for land-atmosphere interaction if snow is shaded by canopy. However, this is inappropriate for snow fully covering short vegetation because z_{0m} should be the snow roughness length ($z_{0m,sn}$) instead of the snow-free ground roughness length in this case.

[36] Potential evapotranspiration is computed from the Penman equation (1a), so the relevant roughness length z_{0m} should be the average z_{0m} for the whole grid cell in Noah. At present, Noah prescribes a vegetation type–dependent roughness length for momentum ($z_{0m,v}$), independent of snow coverage. In our revision, the effective roughness length for the ground is computed as $[(1 - F_{g,sn}^2)\ln z_{0m,g} + F_{g,sn}^2 \ln z_{0m,sn}]$, and then the effective z_{0m} for the grid cell is computed as

$$\ln z_{0m} = \left[\left(1 - F_{g,sn}^2\right)\ln z_{0\,m,g} + F_{g,sn}^2 \ln z_{0m,sn}\right](1 - F_v)^2 + \left[1 - (1 - F_v)^2\right]\ln z_{0\,m,v}, \tag{9}$$

where $z_{0m,g} = 0.01$ m for bare soil, $z_{0m,sn} = 0.001$ m for snow, and the fraction of ground covered with snow ($F_{g,sn}$) is defined in equation (4b). Value F_v is the exposed maximum GVF and is between 0 and 1 as

$$F_v = GVF_{\max} \cdot (1 - F_{\text{bur}}), \tag{10}$$

where F_{bur} is the snow burial fraction in equation (4c), and $GVF_{\max}$ is the maximum GVF prescribed for each grid cell based on satellite data.

[37] In Figure 2, the adjustment of roughness length under snow conditions (Exp. 5) improves the SWE and snow depth simulation a little bit. The effect is more significant over the Valdai grass site (figure not shown).

3.5. Snow Density Adjustment

[38] Noah assumes that 13% of liquid water is stored in snow in the snow density (ρ_{sn}) computation and adjusts ρ_{sn} rapidly to the maximum value of 400 kg/m^3 for $T_1 \ge 0$°C by

$$\rho_{sn} = \rho_{sn}(1 - DW) + DW, \tag{11a}$$

$$DW = 0.13\Delta t/D_{\text{hr}}, \tag{11b}$$

where DW is the portion of liquid water stored in the snowpack during snowmelt, D_{hr} = 24h and Δt is the time step in hours. This leads to an abrupt change of snow density in Noah when surface temperature is near 0°C. To more realistically simulate the ρ_{sn} increase near melting point and to consider the fact that the single temperature (T_1) is used for snow, vegetation, and soil in Noah, we limit the value of DW as

$$DW = \min(DW, 0.13\,M_s/(W + 0.13\,M_s)), \tag{12}$$

where snowmelt M_s is given in equation (3) and W is the SWE. We also use both $T_1 \ge 0$ °C and $T_{\text{soil}(1)} > 0$ °C as conditions for the ρ_{sn} adjustment in equation (11). Figure 2 show that the revision of snow density around 0°C (Exp. 6) does not affect the SWE (Figure 2a) but significantly improves the snow depth simulation compared with observations (Figure 2b).

3.6. Convergence of the Turbulent Exchange Coefficient

[39] The surface exchange coefficient (C_h) is iteratively obtained with no more than five iterations in Noah. However, the C_h fails to converge in the turbulence computation under very stable conditions (figure not shown). After simple sensitivity tests, it is found that C_h would converge if we increase the maximum iteration number from five to 30. Figure 2 indicates that this (i.e., Exp. 7) would improve both SWE and snow depth.

[40] Figure 2 also shows that CLM3.5 simulates SWE and snow depth better than the Noah control run (Exp. 1). The

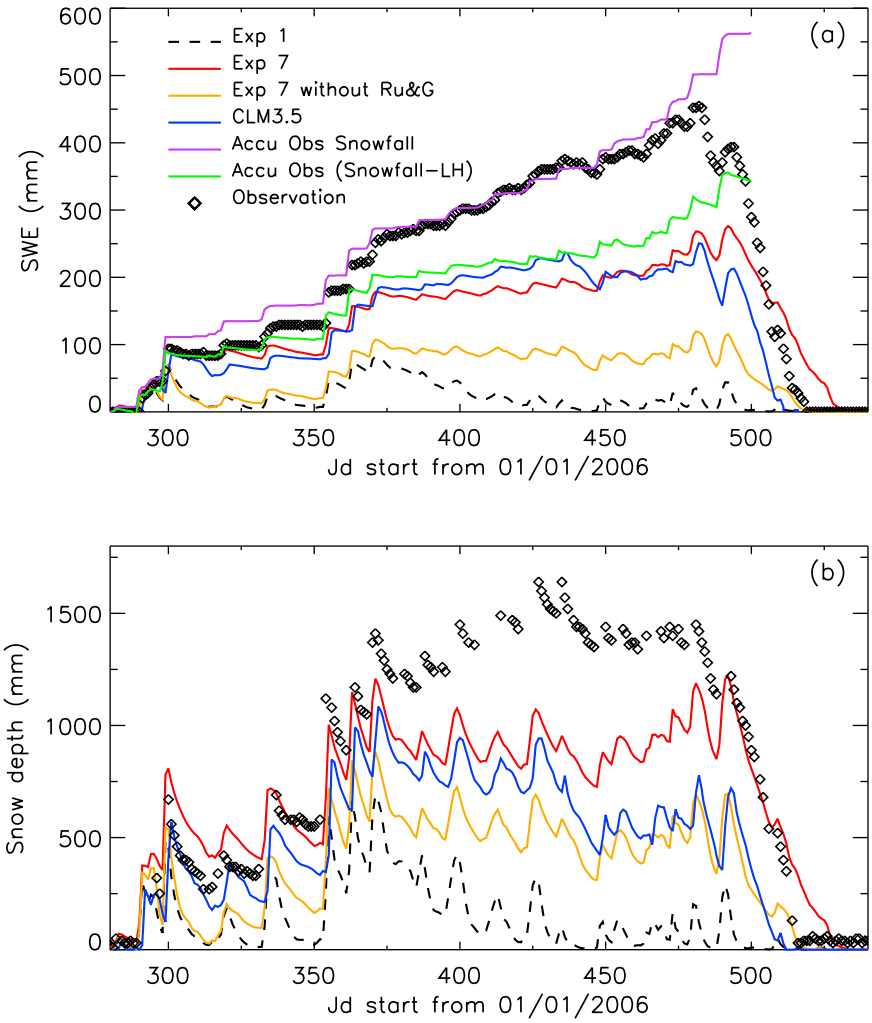

Figure 3. Comparisons of the Noah control (Exp. 1), Noah new run with all revisions (Exp. 7), and NCAR CLM3.5 with observations over the Niwot Ridge site in daily (a) SWE and (b) snow depth. Also shown are the accumulated observed snowfall and accumulated observed snowfall minus latent heat flux as well as the results from Exp. 7 without the under-canopy r_u of equation (6a) and the G adjustment of equation (8).

performance of Noah with all revisions (Exp. 7) in simulating SWE and snow depth is similar to CLM3.5, but is better than CLM3.5 since 1 March 2007.

4. Impact of Our Revisions on Noah Modeling of Snow Processes

4.1. Niwot Ridge Forest Site

[41] Figure 3 shows that the Noah control run (Exp. 1) substantially underestimates SWE and snow depth over the Niwot Ridge forest site in the Colorado Front Range (40.03°N, 105.55°W). Our revisions (Exp. 7) significantly improve the Noah simulation, but the simulated SWE and snow depth are still less than observed values. To explore the reasons for these differences, we also plot the observed accumulated snowfall and the observed accumulated snowfall minus *LH* (green line) in Figure 3a. When the snowmelt is small during the snow accumulation stage, SWE should be close to this green line. Indeed, SWE in Exp. 7 agrees with this green line well in Figure 3a. In contrast, there is a large difference between observed SWE and this green line most of the time. This does not mean that the measurements of SWE, precipitation, and *LH* are wrong; instead it warns that when comparing land model simulated snow variables with observations, we should pay attention to the representativeness of these measurements (particularly over complex terrain).

[42] To further demonstrate the importance of under-canopy resistance in equation (6a) and the G adjustment in equation (8), we also plot Exp. 7 without these two revisions in Figure 3. Evidently, the simulated SWE and snow depth results would degrade without these two revisions.

[43] Besides SWE and snow depth, turbulent flux data are also important in evaluating a land model's performance. Over the Niwot Ridge site, wind speed and temperature fluctuations were measured with a three-dimensional sonic anemometer. Water vapor fluctuations were measured with both an open-path krypton hygrometer and a closed-path infrared gas analyzer [*Turnipseed et al.*, 2004]. Overall, the

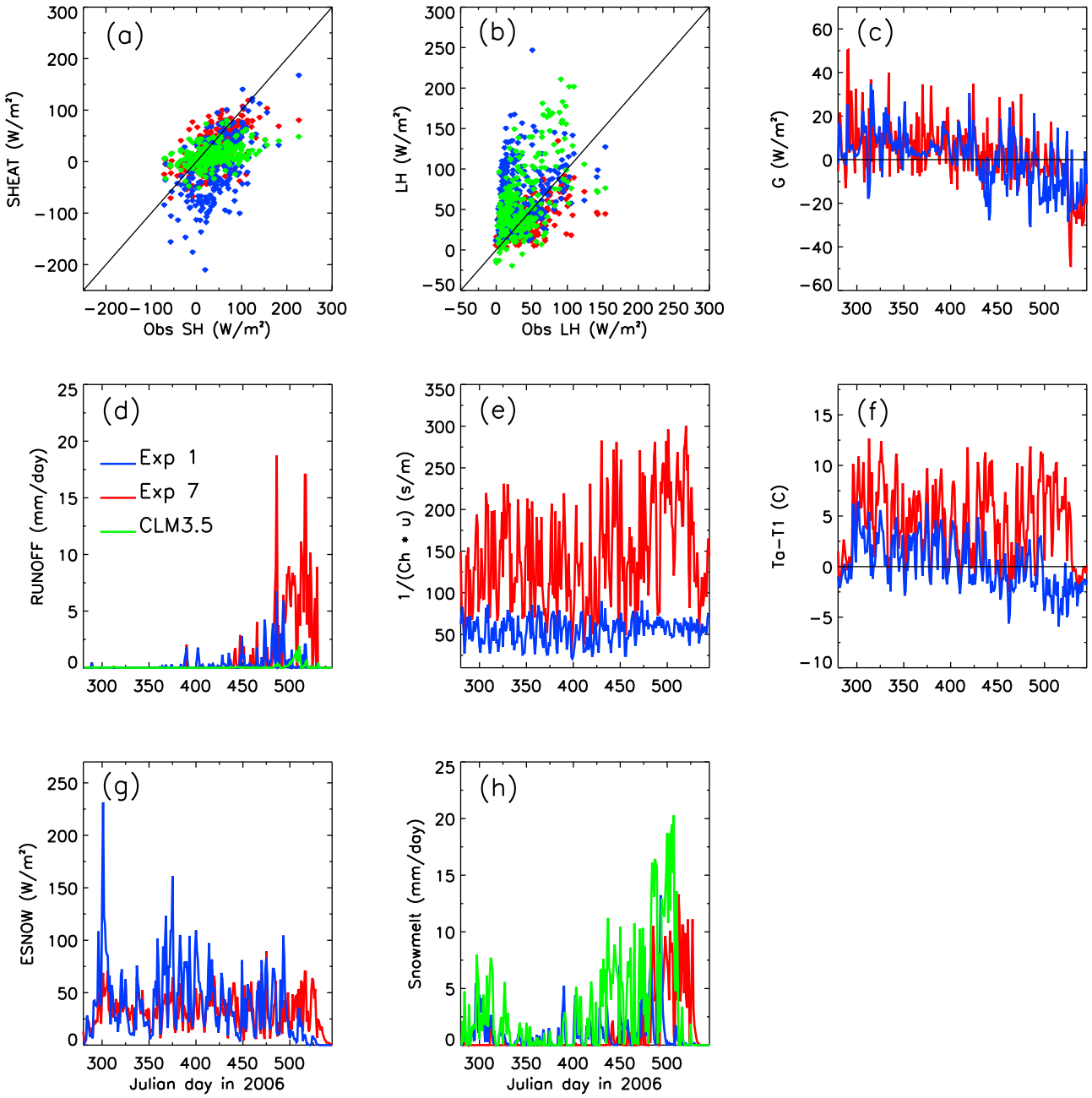

Figure 4. Comparison between the Noah control (Exp. 1), Noah new run with all revisions (Exp. 7), and NCAR CLM3.5 of daily averaged (a) sensible heat flux; (b) latent heat flux; (c) ground heat flux; (d) surface runoff; (e) surface (i.e., aerodynamic and under-canopy) resistance; (f) difference between air and skin temperatures; (g) snow sublimation; and (h) snow melt over the Niwot Ridge site. Observed sensible and latent heat fluxes are also shown in Figures 4a and 4b, respectively.

closed-path system tended to underestimate *LH* by ~3–7% relative to the open-path krypton hygrometer. The only time when instruments did not exhibit good agreement occurred after significant snowfall. During these anomalous periods, only fluxes from the open-path krypton hygrometer were considered valid and used for analysis [*Turnipseed et al.*, 2002, 2004]. Frequent periods of high wind speeds and complicated mountain flow patterns of mountain climates provide a rigorous challenge to eddy flux measurements so that turbulent flux data over complex terrain should be used with caution in land model evaluations.

[44] Figure 4 compares daily averaged variables from Exp. 1 and Exp. 7. Our revisions (Exp. 7) significantly improve the Noah simulation of *SH* and *LH* (Figures 4a and 4b). For example, the correlation and mean absolute deviation between simulated and observed *SH* (or *LH*) are 0.51 (or 0.24) and 50.0 (or 39.1) W/m^2 in the control simulation (Exp. 1), and they are improved to 0.59 (or 0.45)

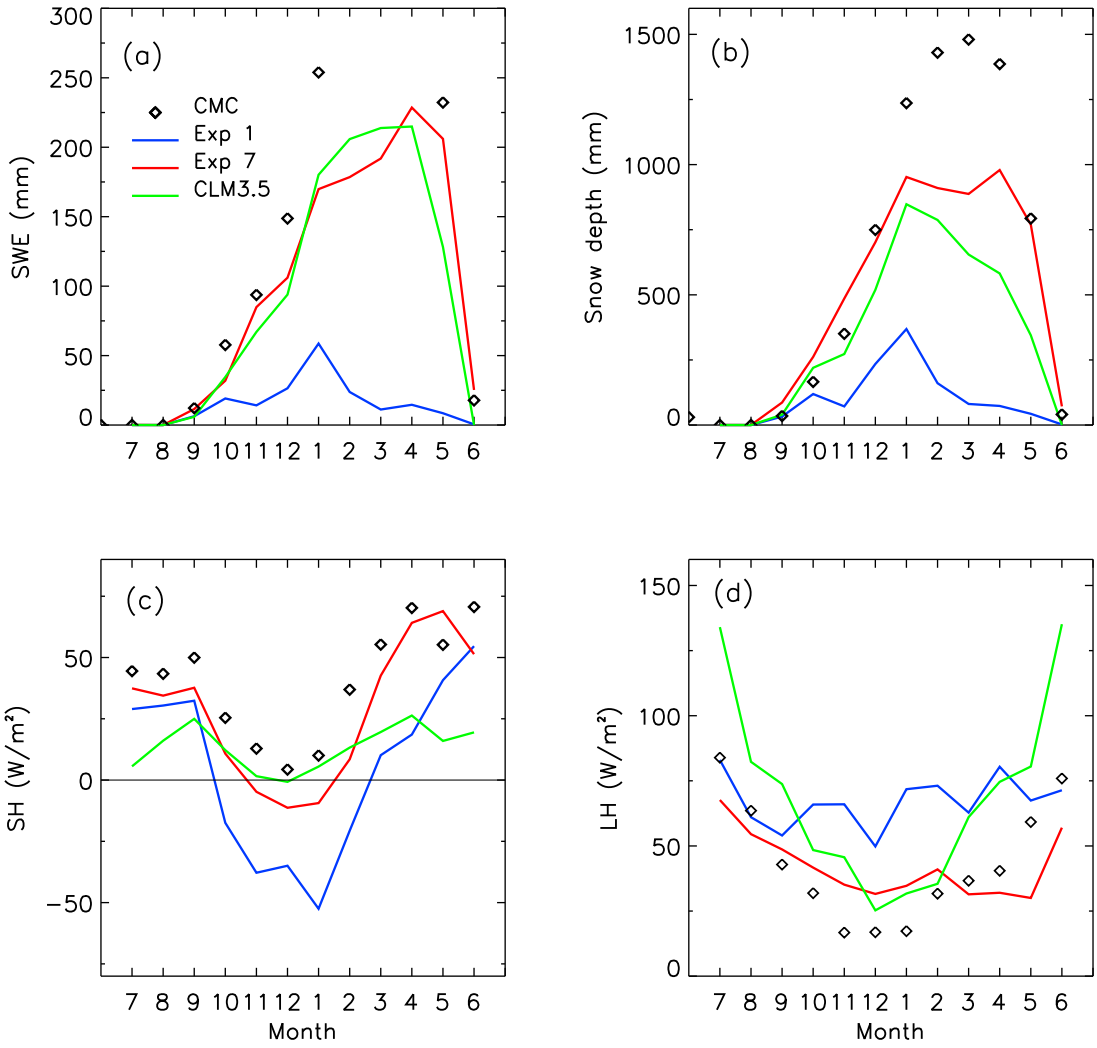

Figure 5. Comparison between the Noah control run (Exp. 1), Noah new run with all revisions (Exp. 7), and NCAR CLM3.5 in monthly averaged (a) SWE; (b) snow depth; (c) sensible heat flux; and (d) latent heat flux from July 2006 to June 2007 over the Niwot Ridge site.

and 30.0 (or 21.5) W/m^2 in Exp. 7, respectively. Our revisions delay the peaks of the surface runoff (Figure 4d), snow sublimation (Figure 4g), and snow melt (Figure 4h), increase surface (aerodynamic and under-canopy) resistance (Figure 4e), and decrease T_1 (or increase $(T_a - T_1)$ in Figure 4f).

[45] The monthly mean values from the Noah control run (Exp. 1), Noah with all revisions (Exp. 7), and NCAR CLM3.5 are evaluated with observations over the Niwot Ridge site in Figure 5. The simulations of SWE, snow depth, *SH*, and *LH* are all significantly improved in Exp. 7 compared with Exp. 1. Both Exp. 7 and CLM3.5 give similar results in SWE (Figure 5a), while Exp. 7 simulates the other three variables better than CLM3.5. CLM3.5 simulates SWE and snow depth better than Exp. 1 (Figures 5a and 5b), but it simulates *SH* and *LH* worse than Exp. 1 (Figures 5c and 5d).

4.2. Boreal Forest Site

[46] As demonstrated in section 4.1, our new revisions improve the Noah simulation of snow processes over the Niwot Ridge forest site. To assess the robustness of our improvements, Figure 6 evaluates the Noah snow simulations over a boreal forest site (53.9°N, 104.7°W). Both Noah with our revisions and CLM3.5 simulate SWE and snow depth better than the Noah control run, and the results from the Noah with our revisions in early spring are better than those from CLM3.5.

[47] Besides SWE and snow depth, we have also analyzed other important variables related to snow processes between the Noah control run (Exp. 1), the new run with all revisions (Exp. 7), and NCAR CLM3.5. Consistent with the increased SWE in Exp. 7 (Figure 6a), the new revisions delay the peak of snow sublimation, snowmelt, and runoff (figure not shown). Reduced sublimation also leads to the decrease of latent heat in springtime in Exp. 7. The overestimate of latent heat in Noah in the spring was also found to be caused by the excessive snow sublimation in the past [*Pan et al.*, 2003; *Slater et al.*, 2007]. The increase of surface (aerodynamic and under-canopy) resistance in Exp. 7 corrects the

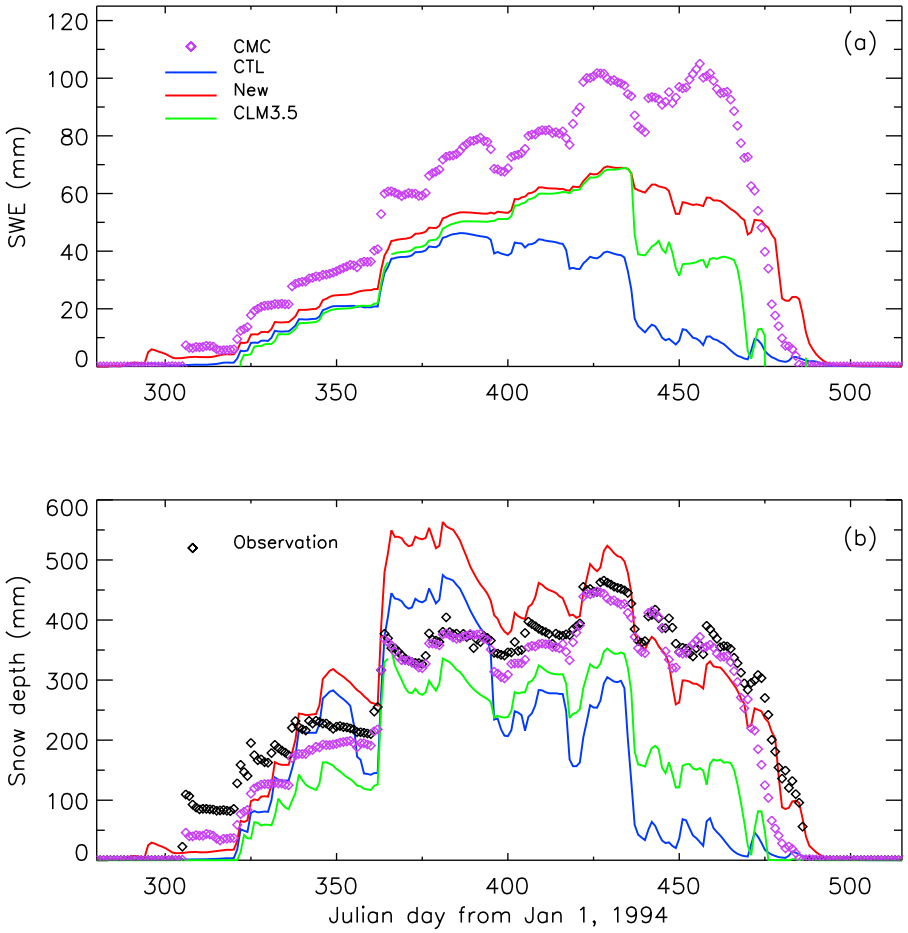

Figure 6. Comparison of daily mean SWE and snow depth over the boreal forest site (53.9°N, 104.7°W) from the Noah control run (CTL), Noah new run with our revisions (new), and NCAR CLM3.5 with observed in situ snow depth data as well as the SWE and snow depth data from the Canadian Meteorological Center (CMC) gridded data set.

excessive downward sensible heat in Noah, which, in turn, decreases the surface skin temperature (figure not shown).

4.3. Fraser Forest Site

[48] Recognizing the challenge in snow modeling in our own efforts and in previous studies, we have also evaluated our revisions, without any tunings, using observational data over the Fraser forest site (39.53°N, 105.53°W).

[49] Figure 7 shows that the Noah control run (Exp. 1) substantially underestimates SWE and snow depth. Both the new run with all revisions (Exp. 7) and CLM3.5 improve SWE and snow depth significantly. In particular, snow essentially disappears at least 1 month earlier in Exp. 1 and 25 days earlier in CLM3.5 than observations, while the timing of snow disappearance is much more reasonable in Exp. 7.

4.4. Valdai Grass Site

[50] Besides the three forest sites, we have also addressed the applicability of our revisions to grass sites where Noah snow simulation is usually not bad [e.g., *Schlosser et al.*, 2000]. For this purpose, Noah with all revisions (Exp. 7) is run without any tunings over the Valdai grass site (57.6°N, 33.1°E).

[51] Figure 8 shows that Noah (Exp. 1) reasonably simulates the seasonal and interannual variability of SWE compared with observations. Our revisions (Exp. 7) further improve the Noah simulation of SWE in most years without degrading the results in any other years.

5. Further Discussions and Conclusions

5.1. Snow Albedo Effect

[52] The early snowmelt problem has been recognized and addressed by various groups from different perspectives. For instance, *Livneh et al.* [2010] reduced Noah's SWE bias by revising the snow albedo formulations, revising the manner in which the snowpack temperature is computed, and including a provision for refreeze of liquid water in the snowpack. Systematic comparison of our revisions and previous revisions, such as those by *Livneh et al.* [2010], is beyond the scope of this study. Here sensitivity tests over two forest sites are done to investigate how the maximum snow albedo ($\alpha_{sn,\max}$) affects the snow simulation. Over the Niwot Ridge site, after increasing $\alpha_{sn,\max}$ from 0.34 to 0.7 and 0.9 in Exp. 1, SWE and snow depth are increased (Figures 9a and 9b) because solar radiation available for snow sublimation and snowmelt is reduced (Figure 9c).

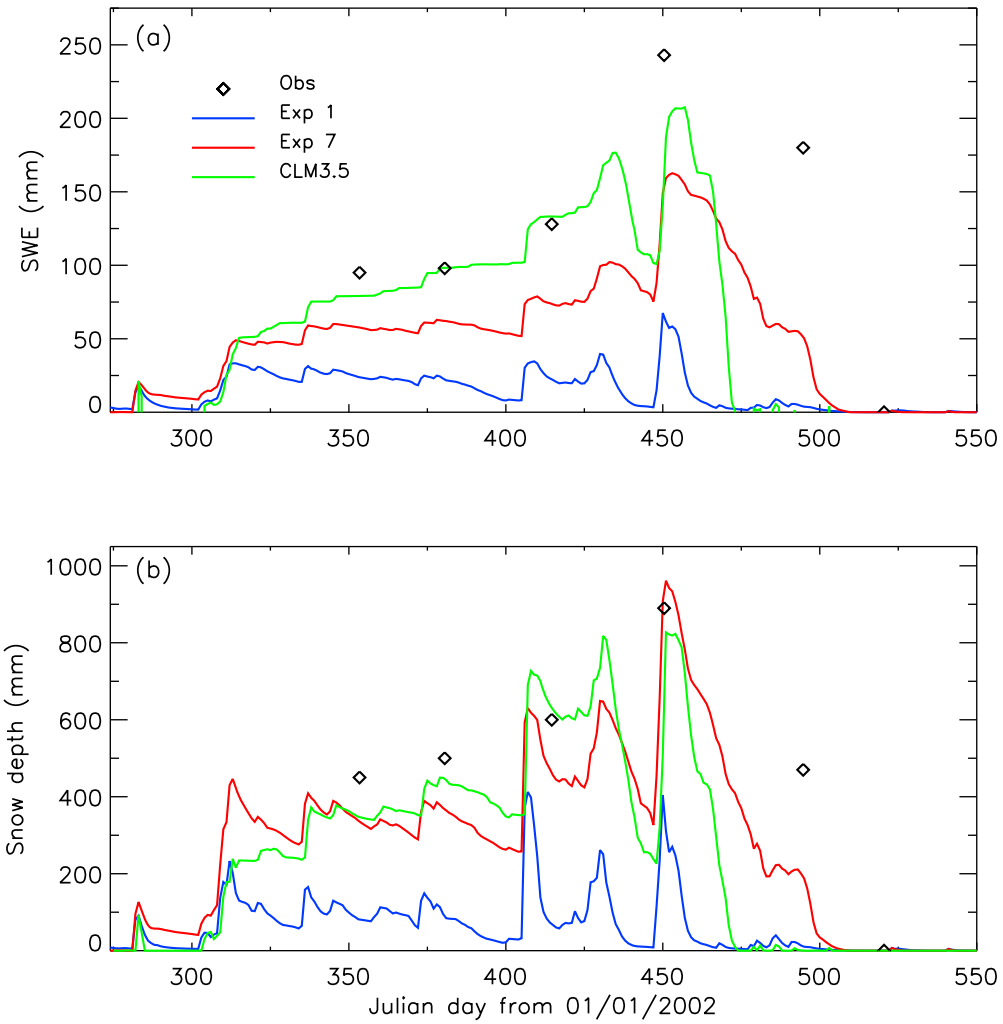

Figure 7. Comparison of the Noah control run (Exp. 1), Noah new run with all revisions (Exp. 7), and NCAR CLM3.5 with observed daily (a) SWE and (b) snow depth over the Fraser forest site (39.53°N, 105.53°W).

However, the simulated SWE and snow depth are still much less than observations. The reduced net radiation associated with a larger $\alpha_{sn,\max} = 0.9$ also reduces both *SH* (Figure 9d) and *LH* (Figure 9e) during the snow and snowmelt season. We have also done sensitivity tests over the Boreal forest site. Results are similar to those in Figure 9, and the early snowmelt problem remains (figure not shown). Therefore increasing snow albedo alone cannot solve the early snowmelt problem of Noah over these two forest sites. Furthermore, it might negatively affect *SH* and *LH*, which are crucial for land-atmosphere coupling.

5.2. Noah Versus CLM3.5

[53] As mentioned earlier, Noah uses a single combined temperature of soil, vegetation, and snow. Our revisions, including the explicit consideration of radiative transfer through canopy, have been made within the Noah modeling structure for easy implementation. An alternative approach might be to substantially revise Noah by changing its structure (e.g., by separately computing vegetation, snow, and ground temperatures, including multilayer snowpacks, and explicitly considering radiative transfer through canopy and snow) (e.g., G. Y. Niu et al., The community Noah land surface model with multi-parameterization (Noah MP) options: 1. Model description and tests at local-scale, manuscript in preparation, 2010). To preliminarily address this issue, we compare our results with those from a more complicated and continuously improving land model, i.e., the Community Land Model (CLM3.5) [*Oleson et al.*, 2008]. We focus on the three forest sites because the complicated vegetation structure in CLM3.5 affects snow simulation over tall vegetation much more than that over short vegetation. Over the Niwot Ridge site, both CLM3.5 and our revisions (Exp. 7) can capture the snowpack features better than the Noah control run (Figures 2 and 3). Exp. 7 is slightly better than CLM3.5 in simulating snow depth (Figures 2b and 3b). Over the boreal forest site, CLM3.5 simulates snow processes better than the Noah control run (Exp. 1) (Figure 6), but it still has an early snowmelt problem (Figure 6a). Similarly, over the Fraser forest site, CLM3.5 simulates the snow process better than Noah (Exp. 1) (Figure 7). CLM3.5-simulated SWE is closer to observations than that in Exp. 7 (Figure 7a), but our revisions (Exp. 7) capture the snowmelt timing much better than CLM3.5. Therefore Noah with our revisions (Exp. 7)

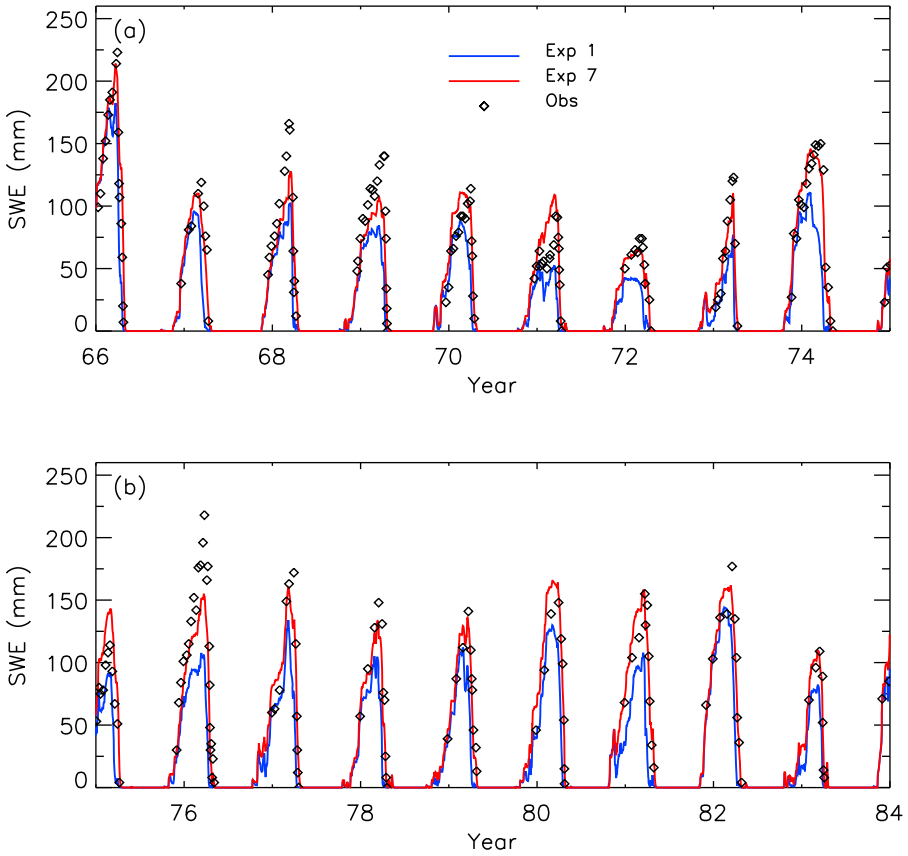

Figure 8. Comparison of the Noah control run (Exp. 1) and the Noah new run with all revisions (Exp. 7) with observed daily SWE over the Valdai grassland site (57.6°N, 33.1°E) from (a) 1966–1974 and (b) 1975–1983.

can perform as well as, or slightly better than, CLM3.5 at these three sites.

5.3. Conclusions

[54] Snow is one of the most crucial land surface processes over middle and high latitudes. Early snowmelt is a well-recognized deficiency of the Noah land model as used in NCEP operational models and the WRF research model. Various groups have attempted to address this challenging issue. Complementary to these efforts, we have done detailed diagnostics of the Noah output over a high-altitude midlatitude forest site and a boreal forest site. Six deficiencies in Noah model physics are identified along with revised formulations to remove these deficiencies by (1) considering the vegetation shading effect on snow sublimation and melt; (2) considering under-canopy resistance; (3) revising the ground heat flux computation; (4) revising the momentum roughness length computation under snow conditions; (5) revising the snow density computation near 0°C; and (6) increasing the maximum iteration number from five to 30 in the turbulence computation.

[55] Comparisons with the observational data over the Niwot Ridge forest site (40.03°N, 105.55°W) and the boreal forest site (53.9°N, 104.7°W) demonstrate that these revisions indeed improve the Noah simulations of all snow processes such as snow water equivalent (SWE), snow depth, as well as sensible and latent heat fluxes. In particular, consideration of the canopy shading effect of the underlying snow is most important for the overall snow simulation, while the adjustment of the snow density near 0°C is important for the snow depth simulation. Other revisions are important for specific periods. For instance, increasing the maximum iteration number from five to 30 helps the convergence of the turbulent computation only under very stable conditions (because five iterations are enough for convergence under other conditions).

[56] Tests of our revisions, without any tunings, have also been done over an independent high-altitude midlatitude forest site, i.e., the Fraser forest site (39.53°N, 105.53°W), and confirm that our revisions indeed improve the Noah simulation of snow processes. While our revisions are primarily relevant to forest regions with underlying snow, it is also important to verify whether the good performance of Noah in simulating snow over short vegetation is affected positively or negatively. Therefore we also tested our revisions over the Valdai grassland site (57.6°N, 33.1°E) without any tunings and found that our revisions improve the SWE simulation in some years and do not degrade the Noah simulation in any other years.

[57] Our revisions maintain the Noah model structure and do not introduce new prognostic variables for easy implementation into NCEP operational models and into WRF, and they explicitly consider the radiative transfer through canopy. An alternative approach is to significantly change the Noah model structure, as attempted by Niu et al. (manuscript in preparation, 2010). As an initial step, we

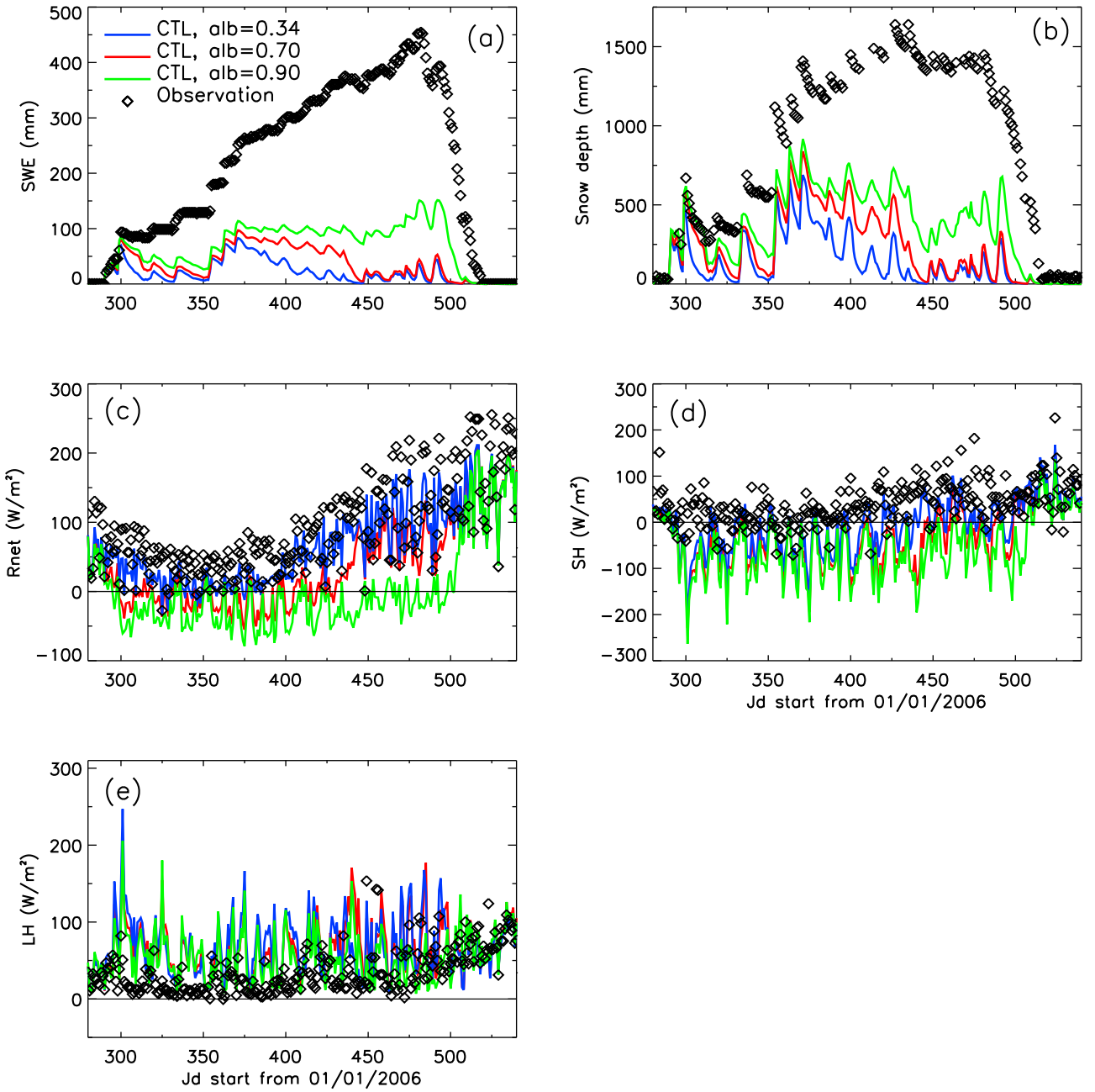

Figure 9. Sensitivity of the Noah model (Exp. 1) to maximum snow albedo $\alpha_{sn,\max}$ values of 0.34 (control), 0.70, and 0.9 over the Niwot Ridge site. (a) daily SWE; (b) snow depth; (c) net radiation; (d) *SH*; and (e) *LH*.

have also preliminarily compared the default Noah, Noah with our revisions, and CLM3.5 which has a much more complicated structure for snow, vegetation, and soil. It is found that CLM3.5 performs better than the default Noah, but Noah with our revisions is as good as, or slightly better than, CLM3.5 in the snow simulation over the three forest sites.

[58] As a sensitivity test, we have also preliminarily evaluated the effect of increasing the maximum snow albedo (from 0.34 to 0.9), as suggested in some previous studies, on the Noah snow simulations. It does slightly increase SWE and snow depth simulation accuracy due to the decrease of the available solar radiation for snowmelt in Noah over the Niwot Ridge and boreal forest sites. However, the overall early snowmelt problem of Noah remains. Furthermore, the decrease of the available solar radiation also reduces both sensible and latent heat fluxes, both of which are crucial for atmospheric boundary layer processes.

[59] In the process of evaluating model results using observational data, it is also found that observational SWE is higher than the observational snowfall minus latent heat flux over the Niwot Ridge site (e.g., due to the horizontal wind-blowing of snow). Therefore special attention should be paid to the representativeness of the snow measure-

ments (particularly over complex terrain) in evaluating land models.

[60] Further tests are needed to assess the regional and global applicability of our revisions in Noah. More detailed comparisons of our revisions with previous efforts (with or without changing the Noah model structure) are also needed. These will be our future tasks in collaboration with various partners.

[61] **Acknowledgments.** This work is supported by NOAA (NA07NES4400002), NSF (ATM−0634762), and NASA (NNX09A021G). Michael Brunke's help in improving the readability of the manuscript is appreciated. We especially thank three reviewers for detailed and insightful comments, which helped improve the clarity of our presentation. We also wish to thank Russ Monson, the principal investigator of the Niwot Ridge Ameriflux data.

References

Anderson, E. A. (1976), A point energy and mass balance model of a snow cover, *NOAA Tech. Rep. NWS 19*, 50 pp., *Off. of Hydrol., Natl. Weather Serv.*, Natl. Oceanic and Atmos. Admin., Silver Spring, Md.

Barry, R. (1973), A climatological transect on the east slope of the Front Range, Colorado, *Arc. Alp. Res.*, *5*, 89–110.

Betts, A. K., and J. H. Ball (1997), Albedo over the boreal forest, *J. Geophys. Res.*, *102*, 28,901–28,909, doi:10.1029/96JD03876.

Boone, A., et al. (2004), The Rhone-aggregation land surface scheme intercomparison project: An overview, *J. Clim.*, *17*, 187–208.

Bowling, L. C., et al. (2003), Simulation of high-latitude hydrological processes in the Torne-Kalix basin-PILPS Phase 2 (e) 1: Experiment description and summary intercomparisons, *Global Planet. Change*, *38*, 1–30, doi:10.1016/S0921-8181(03)00003-1.

Brasnett, B. (1999), A global analysis of snow depth for numerical weather prediction, *J. Appl. Meteorol.*, *38*, 726–740.

Brazel, A., and P. Brazel (1983), Summer diurnal wind patterns at Niwot Ridge, CO, *Phys. Geogr.*, *4*, 53–61.

Brown, R. D., B. Brasnett, and D. Robinson (2003), Gridded North American monthly snow depth and snow water equivalent for GCM evaluation, *Atmos. Ocean*, *41*, 1–14.

Chen, F., and J. Dudhia (2001), Coupling an advanced land surface-hydrology model with the Penn State-NCAR MM5 modeling system: part I. Model implementation and sensitivity, *Mon. Weather Rev.*, *129*, 569–585.

Chen, F., et al. (1996), Modeling of land surface evaporation by four schemes and comparisons with FIFE observations, *J. Geophys. Res.*, *101*, 7251–7268, doi:10.1029/95JD02165.

Chen, F., Z. Janjic, and K. Mitchell (1997), Impact of atmospheric surface-layer parameterizations in the new land-surface scheme of the NCEP mesoscale ETA model, *Boundary Layer Meteorol.*, *85*, 391–421, doi:10.1023/A:1000531001463.

Cline, D. W. (1996), Effect of seasonality of snow accumulation and melt on snow surface energy exchanges at a continental alpine site, *J. Appl. Meteorol.*, *36*, 32–51.

Cline, D., R. Armstrong, R. Davis, K. Elder, and G. Liston (2004), CLPX main met snow pit measurements, edited by Parsons, M. and M. J. Brodzik, in *CLPX−Ground: ISA Main Meteorological Data*, edited by K. Elder and A. Goodbody, Natl. Snow and Ice Data Cent., Boulder, Colo.

Collins, W. D., et al. (2006), The community climate system model version 3 (CCSM3), *J. Clim.*, *19*, 2122–2143.

Dai, Y., et al. (2003), The common land model (CLM), *Bull. Am. Meteorol. Soc.*, *84*, 1013–1023.

Decker, M., and X. Zeng (2009), Impact of modified Richards equation on global soil moisture simulation in the Community Land Model (CLM3.5), *J. Adv. Model. Earth Syst.*, *1*, Art. 5, 22 pp., doi:10.3894/JAMES.2009.1.5.

Ek, M., K. Mitchell, Y. Lin, E. Rogers, P. Grunmann, V. Koren, G. Gayno, and J. Tarpley (2003), Implementation of Noah land surface model advances in the National Centers for Environmental Prediction operational mesoscale Eta model, *J. Geophys. Res.*, *108*(D22), 8851, doi:10.1029/2002JD003296.

Elder, K., and A. Goodbody (2004), CLPX-Ground: ISA main meteorological data, Natl. Snow and Ice Data Cent., Boulder, Colo.

Essery, R., et al. (2009), SNOWMIP2—An evaluation of forest snow process simulations, *Bull. Am. Meteorol. Soc.*, *90*, 1120–1135.

Etchevers, P., et al. (2004), Validation of the energy budget of an alpine snowpack simulated by several snow models (SnowMIP project), *Ann. Glaciol.*, *38*, 150–158.

Feng, X., A. Sahoo, K. Arsenault, P. Houser, Y. Luo, and T. Troy (2008), The impact of snow model complexity at three CLPX sites, *J. Hydrometeorol.*, *9*, 1464–1481.

Frei, A., and D. A. Robinson (1998), Evaluation of snow extent and its variability in the Atmospheric Model Intercomparison Project, *J. Geophys. Res.*, *103*, 8859–8871, doi:10.1029/98JD00109.

Frei, A., R. Brown, J. A. Miller, and D. A. Robinson (2005), Snow mass over North America: Observations and results from the second phase of the atmospheric model intercomparison project, *J. Hydrometeorol.*, *6*, 681–695, doi:10.1175/JHM443.1.

Hollinger, D. Y., and S. C. Wofsy (1997), Science plan for AmeriFlux: Long-term flux measurement network of the Americas, AmeriFlux, Oak Ridge, Tenn.

Jin, J., and N. L. Miller (2007), Analysis of the impact of snow on daily weather variability in mountainous regions using MM5, *J. Hydrometeorol.*, *8*, 245–258.

Jin, J., X. Gao, Z.-L. Yang, R. C. Bales, S. Sorooshian, R. E. Dickinson, S.-F. Sun, and G.-X. Wu (1999), Comparative analyses of physically based snowmelt models for climate simulations, *J. Clim.*, *12*, 2643–2657.

Jordan, R. (1991), A one-dimensional temperature model for a snow cover, *CREEL Spec. Rep. 91–16*, Cold Reg. Res. and Eng. Lab. U.S. Army Corps of Eng., Hanover, N. H.

Koren, V., J. C. Schaake, K. E. Mitchell, Q. Y. Duan, F. Chen, and J. Baker (1999), A parameterization of snowpack and frozen ground intended for NCEP weather and climate models, *J. Geophys. Res.*, *104*, 19,569–19,585, doi:10.1029/1999JD900232.

Lawrence, P. J., and T. N. Chase (2009), Climate impacts of making evapotranspiration in the Community Land Model (CLM3) consistent with the Simple Biosphere Model (SiB), *J. Hydrometeorol.*, *10*, 374–394.

Livneh, B., Y. L. Xia, K. Mitchell, M. Ek, and D. P. Lettenmaier (2010), Noah LSM snow model diagnostics and enhancements, *J. Hydrometeorol.*, *11*, 721–738, doi:10.1175/2009JHM1174.1.

Mahrt, L., and H.-L. Pan (1984), A two-layer model of soil hydrology, *Boundary Layer Meteorol.*, *29*, 1–20.

Mahrt, L., and M. Ek (1984), The influence of atmospheric stability on potential evaporation, *J. Clim. Appl. Meteorol.*, *23*, 222–234.

Mitchell, K., et al. (2004), The multi-institution North American Land Data Assimilation System (NLDAS): Utilizing multiple GCIP products and partners in a continental distributed hydrological modeling system, *J. Geophys. Res.*, *109*, D07S90, doi:10.1029/2003JD003823.

Monson, R. K., et al. (2002), Carbon sequestration in a high-elevation subalpine forest, *Global Change Biol.*, *8*, 1–20.

Mote, T. L., A. J. Grundstein, D. J. Leathers, and D. A. Robinson (2003), A comparison of modeled, remotely sensed, and measured snow water equivalent in the northern Great Plains, *Water Resour. Res.*, *39*(8), 1209, doi:10.1029/2002WR001782.

Niu, G. Y., and Z. L. Yang (2007), An observation-based formulation of snow cover fraction and its evaluation over large North American river basins, *J. Geophys. Res.*, *112*, D21101, doi:10.1029/2007JD008674.

Oleson, K. W., et al. (2004), Technical description of the community land model (CLM), *NCAR/TN-461+STR*, Natl. Cent. for Atmos. Res., Boulder, Colo.

Oleson, K. W., et al. (2008), Improvements to the Community Land Model and their impact on the hydrological cycle, *J. Geophys. Res.*, *113*, G01021, doi:10.1029/2007JG000563.

Pan, M., et al. (2003), Snow process modeling in the North American Land Data Assimilation System (NLDAS): 2. Evaluation of model-simulated snow water equivalent, *J. Geophys. Res.*, *108*(D22), 8850, doi:10.1029/2003JD003994.

Parrish, D. D., et al. (1990), Systematic variations in the concentration of NO_x (NO + NO_2) at Niwot Ridge, Colorado, *J. Geophys. Res.*, *95*, 1817–1836.

Penman, H. L. (1948), Natural evaporation from open water, bare soil, and grass, *Proc. R. Soc. London, Ser. A*, *193*, 120–195.

Qu, X., and A. Hall (2006), Assessing snow albedo feedback in simulated climate change, *J. Clim.*, *19*, 2617–2630, doi:10.1175/JCLI3750.1.

Rutter, N., et al. (2009), Evaluation of forest snow processes models (SnowMIP2), *J. Geophys. Res.*, *114*, D06111, doi:10.1029/2008JD011063.

Sakaguchi, K., and X. Zeng (2009), Effects of soil wetness, plant litter, and under-canopy atmospheric stability on ground evaporation in the Community Land Model (CLM3.5), *J. Geophys. Res.*, *114*, D01107, doi:10.1029/2008JD010834.

Schlosser, C. A., et al. (2000), Simulations of a boreal grassland hydrology at Valdai, Russia: PILPS Phase 2(d), *Mon. Weather Rev.*, *128*, 301–321.

Sellers, P. J., et al. (1997), BOREAS in 1997: Experiment overview, scientific results, and future directions, *J. Geophys. Res.*, *102*, 28,731–28,769, doi:10.1029/97JD03300.

Sheffield, J., et al. (2003), Snow process modeling in the North American Land Data Assimilation System (NLDAS): 1. Evaluation of model-simulated snow cover extent, *J. Geophys. Res.*, *108*(D22), 8849, doi:10.1029/2002JD003274.

Shewchuk, S. R. (1997), Surface mesonet for BOREAS, *J. Geophys. Res.*, *102*, 29,077–29,082, doi:10.1029/96JD03875.

Slater, A. G., et al. (2001), The representation of snow in land surface schemes: Results from PILPS 2(d), *J. Hydrometeorol.*, *2*, 7–25.

Slater, A. G., T. J. Bohn, J. L. McCreight, M. C. Serreze, and D. P. Lettenmaier (2007), A multimodel simulation of pan-Arctic hydrology, *J. Geophys. Res.*, *112*, G04S45, doi:10.1029/2006JG000303.

Turnipseed, A. A., P. D. Blanken, D. E. Anderson, and R. K. Monson (2002), Energy budget above a high-elevation subalpine forest in complex topography, *Agric. For. Meteorol.*, *110*, 177–201, doi:10.1016/S0168-1923(01)00290-8.

Turnipseed, A. A., D. E. Anderson, P. D. Blamken, W. Baugh, R. K. Monson (2003), Airflows and turbulent flux measurements in mountainous terrain: part 1. Canopy and local effects, *Agric. For. Meteorol.*, *119*, 1–21, doi:10.1016/S0168-1923(03)00136-9.

Turnipseed, A. A., D. E. Anderson, S. Burns, P. D. Blanken, and R. K. Monson (2004), Airflows and turbulent flux measurements in mountainous terrain: part 2. Mesoscale effects, *Agric. For. Meteorol.*, *125*, 187–205, doi:10.1016/j.agrformet.2004.04.007.

Vernekar, A. D., J. Zhou, and J. Shukla (1995), The effect of Eurasian snow cover on the Indian monsoon, *J. Clim.*, *8*, 248–266.

Vinnikov, K. Y., A. Robock, N. A. Speranskaya, and C. A. Scholosser (1996), Scale of temporal and spatial variability of midlatitude soil moisture, *J. Geophys. Res.*, *101*, 7163–7174, doi:10.1029/95JD02753.

Wang, A. H., and X. Zeng (2009), Improving the treatment of the vertical snow burial fraction over short vegetation in the NCAR CLM3, *Adv. Atmos. Sci.*, *26*, 877–886, doi:10.1007/s00376-009-8098-3.

Wang, Z., and X. Zeng (2010), Evaluation of snow albedo in land models for weather and climate studies, *J. Appl. Meteorol. Clim.*, *49*, 363–380, doi:10.1175/2009JAMC2134.1.

Wang, Z., X. Zeng, M. Barlage, R. E. Dickinson, F. Gao, and C. B. Schaaf (2004), Using MODIS BRDF and albedo data to evaluate global model and land surface albedo, *J. Hydrometeorol.*, *5*, 3–14.

Williams, M. W., T. Bardsley, and M. Rikkers (1998), Overestimation of snow depth and inorganic nitrogen wetfall using NADP data, Niwot Ridge, Colorado, *Atmos. Environ.*, *32*, 3827–3833.

World Meteorological Organization (1986), Intercomparison of models of snowmelt runoff, *WMO Ser.*, *646*, 440 pp., World Meteorol. Organ., Geneva, Switzerland.

M. Decker, Z. Wang, and X. Zeng, Department of Atmospheric Sciences, University of Arizona, 1118 E. 4th St., PO Box 210081, Tucson, AZ 85721-0081, USA. (zhuowang@atmo.arizona.edu)